

Sensorimotor Learning of a Virtual Skill

Spencer R. Wilson

March 10, 2021

1 Introduction & Aims

Movement is nothing but the quality of our being.

— Sunryu Suzuki, *Zen Mind, Beginner’s Mind*

The purpose of this thesis is to construct a high-dimensional electromyography recording setup as a platform on which a suite of motor control and learning experiments can be explored. With this novel setup, we hope to advance our understanding of trial-to-trial motor learning through the combination of experiment and theory.

A recent review provides a clear call to action for work this direction:

The processes by which biological control solutions spanning large and continuous state spaces are constructed remain relatively unexplored. Future investigations may need to embed rich dynamical interactions between object dynamics and task goals in novel and complex movements.¹

Over the last few decades, there has been considerable amount of work done to untangle the abilities of the motor system to flexibly control the body including through optimal control theory², reinforcement learning in continuous action space³, and detailed physiological studies⁴. However, as the quote above suggests, a holistic understanding of the computations underlying the construction of skilled movement remains an exciting direction for research. Our aim is to progress understanding of skilled movement by studying the solutions produced by human subjects to motor tasks in dynamically rich, yet controlled, virtual environments. Our goal is to reverse-engineer the ability to acquire and perform novel motor skills.

Humans produce a great variety of movements every day, often without conscious thought. For example, movements like bringing a cup of coffee to our lips for a sip are generally out of reach for state-of-the-art robotic systems. We claim that this “motor gap” between biological and artificial motor systems is due to a lack of *dexterity*. Soviet neuroscientist Nikolai Bernstein defined dexterity as the ability to “find a motor solution in any situation and in any condition.”⁵ The crux of this definition is the flexibility of such solutions. This flexibility, or robustness¹⁶, is the ability to optimize internal parameters in response to external perturbations and adapt to new information to achieve the goals of an ongoing plan.

To explore dexterous movement, we will leverage recordings of muscles controlling the hand as a readout of flexible motor behavior. This is a step beyond recording hand kinematics as electromyography provides a physiological output of the nervous system. Surface electromyography recordings taken from the forearms controlling subjects’ dominant hands allows us to track the sequential selection of muscle activations during both skill acquisition and subsequent performance of that skill to achieve desired goal. As we are interested in subjects’ abilities to acquire new skills, we design tasks that require subjects to use available, but uncommon, motor activations. We then

¹Kitano defines robustness as “the maintenance of specific functionalities of the system against perturbations, and it often requires the system to change its mode of operation in a flexible way.” He claims that robustness requires control, alternative mechanisms, modularity and decoupling between high and low level variability.

track the selection and execution of these activation during virtual tasks. Preliminary work in this direction is described in Section 3.

Using data from our experimental setup, we wish to understand both how the structure of muscle activation variability evolves during skill acquisition and how the motor system constructs skilled movement through the composition of component muscle activations. To begin, we review a sampling of current motor physiology research relevant to dexterous motor computations in Section 2. In Section 3, we cover our prototype hardware and experiments. With inspiration from physiology and our experiments, we hope to make progress in modeling sensorimotor control and learning in our experimental setup. We cover preliminary work in this direction in Section 4, and discuss possible future directions in Section 5.

2 Reverse Engineering the Movement Machine

Even a simple movement is a global body event.

— Bizzi & Ajemian, 2020

2.1 Motor Units to Muscles

The quantum of motor output is the motor unit (MU), defined as a single motoneuron axon and the set of junctions the terminals of its axon branches form with one or more muscle fibers. The MU provides the motor system with spatial redundancy at the muscle level: multiple muscle fibers contract due to a single alpha motoneuron (AMN) spike in the spinal cord’s ventral horn, and multiple AMNs may overlap in their innervations. The forces produced by motor units span several orders of magnitude, though most units produce very small forces. Here we find temporal redundancy: in order to produce movements, MUs combine to generate a range of forces⁷. Since the innervation ratios of muscles in the forearm and hand are relatively small compared to more proximal muscles (which contain thousands of MUs), the logarithmic recruitment and redundancy of motor units enables the hand to produce movements with very fine spatiotemporal resolution.

Muscle fibers are contained within muscle compartments, and each muscle may have one or more compartments. The fingers of the hand are extended by the extensor digitorum (ED) which contains four compartments, one for each of the tendons the muscle produces. Each tendon connects to the three metaphalangeal joints of each digit. The fingers are flexed by two muscles, the flexor digitorum superficialis (FDS) and the flexor digitorum profundus (FDP). Like the ED, these muscles produce four tendons, one to each finger from each of their four compartments. As such, one must coactivate these agonist and antagonist muscles in order to extend or flex a single finger in isolation⁷. Adduction and abduction of the fingers is produced by the 19 intrinsic muscles of the hand, each of which has their origin and insertion points within the hand itself⁸. The intrinsic muscle tendons form a kind of network around each of the digits. The human hand, thumb, and forearm system contains more than 30 muscles and at least 20 degrees of freedom are theoretically available for actuation. However, due to biomechanical coupling, the effective degrees of freedom is presumably less than 20.

This structure exists in order to facilitate the acquisition of new skills and the generalization of existing skills to new contexts. While the anatomy of the hand and forearm presents constraints on movement, the system remains capable of producing an incredible variety of movement patterns^{9,102}. The structure of the neuromuscular system that underlies this variety offers many clues as to the relevant computations required for dexterous movement. In Fig. 1, Yan et al. show how even low-variance principle components of joint kinematics during object grasping and ASL signing display correlational structure and not merely noise. That is, the production of hand movement is highly task-specific, where individual tasks are linked to bespoke muscle activations patterns.

2.2 Coordinative Structures

Many studies have contributed to the concept of synergies as a hard-wired organizing feature of the motor system¹¹. However, these works tend to extrapolate from non-primate preparations, particularly in the frog, and use tasks which are inherently low-dimensional to explain covariance structure in primate and human kinematic and electromyography data^{12,13}. That said, it would be foolish to deny the existence of synergistic muscle coactivation even at the structural level. Careful studies of force control by the fingertips present a complex story of dimensionality of control in this regime¹⁴. Constraints exist in the architecture of the hand as well as its control system, though we maintain that concept of synergies, especially in the context of dexterous movement, is often presented as an oversimplification rather than a mere simplification. We believe the story of the hand is more complex.

²In a classic study, Basmajian and colleagues showed that it is possible to activate single motor units in the thumb abductor.

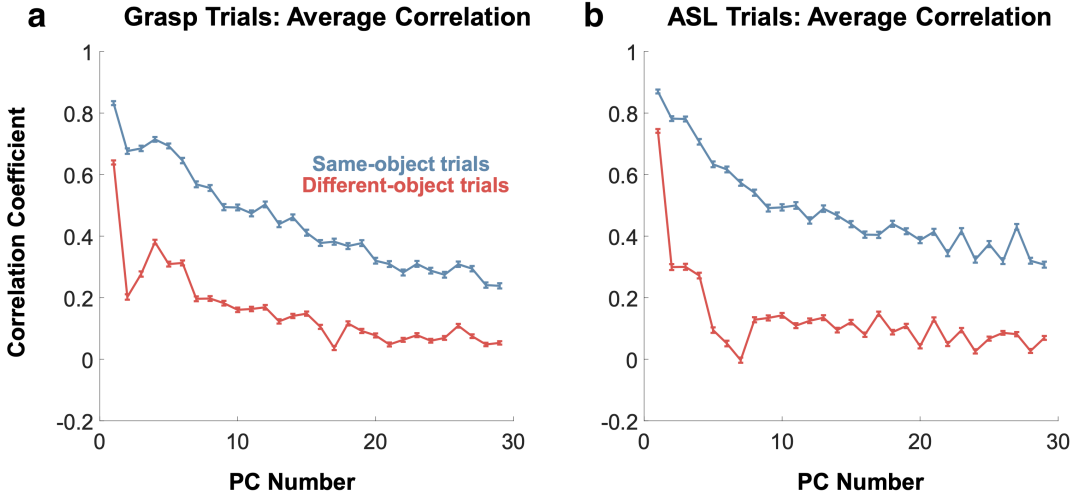


Figure 1: Taken from Yan et al. 2020. Plots show mean correlations between hand joint kinematic trajectories during grasp trials with the same (blue) and different (red) objects (a) and ASL signs (b) projected onto the same principle components. Correlations are averaged across 8 subjects. Within-object and within-sign correlations are systematically higher than their shuffled counterparts. Error bars denote SEM. This data supports the idea that low-variance components of kinematics data contain task-specific structure rather than merely reflecting noise. This is encouraging for our experiments, which hope to extend this idea into careful analyses of task specific features of EMG data across learning and in response to perturbations.

Studies have attempted to quantify the number of effective degrees of freedom of the hand with various methods. This has primarily been taken to be the number of linear features which contain a desired level of the original signal variance, where the signal is the joint angles of the hand engaged in various behaviors^{15,16}. These methods have resulted in roughly 8 linear features of hand kinematics to solve a variety of tasks, with subtleties found in inter-task and inter-subject variations. Note that the motor repertoire is hardly high-dimensional when compared to the dimensionality of the visual feature extraction system⁹. A recent study found that low-variance linear, kinematic components displayed significantly higher correlation within condition (e.g. grasp of a specific object) than across condition. This suggests that these components carry task-dependent information rather than condition-independent, task-irrelevant noise⁹. This suggests that the control of the hand is more nuanced than a set of fixed synergies.

What Bizzi and colleagues call “the problem of supraspinal pattern formation”—how synergies are activated through time— we argue, in the context of hand control, is not simplified by the existence of hard-wired or soft-wired synergies¹⁷. Rather, the CNS produces control signals in a range of contexts and in response to continually changing task demands. **Rather than the CNS “simplifying movement” through synergetic action, it is more likely that hand synergies fall out of a optimization strategy which trades off effort and accuracy where effort may, in part, correspond to independent control of individual control dimensions.** In this view, synergies, hard-wired or not, reflect the statistics of the environment in which movement is constructed¹⁸. If we limit ourselves to synergetic control, then we have simply passed the problem to a lower-dimensional one of the same fundamental nature. Neural control of the hand likely contains a spectrum of modularity in order to maintain its role as a flexible instrument. Synergetic action is one end of this spectrum resulting from the computations inherent to, along with the structures of the human movement machine.

2.3 Fractionating Structures

Just as many muscle fibers may be innervated by a single AMN, up to thousands of neurons contact single AMNs through monosynaptic corticospinal, or corticomotoneuronal (CM), connections and other descending pathways through elaborate spinal circuitry. The hallmark of CM connections in particular is their influence over multiple muscle compartments as well as multiple muscles, though typically agonist or antagonist sets¹⁹. This may seem counter-intuitive as a means to produce individuated movement, but experimental evidence in primates has shown that the convergence of many CM collateral fibers onto single AMNs driving the distal muscles in particular can produce a fine grading of activity over motor units driving the distal joints. CM cells also appear to play a role in the inhibition of antagonist muscles prior to contractions required for movement.²⁰ These findings confirm theories about the excitatory and inhibitory role of these connections dating back decades, and combine to suggest that variables encoded in cortical ensembles are more complex than kinematics or dynamics alone¹⁹.

The CM tract thus acts in coordination with synergistic muscle activations of the hand to achieve control that is balanced between modularity and flexibility. Findings suggest that there is a bipartite structure in human motor cortex driving dexterous control of the distal part of the upper limb which, it has been suggested, evolved under pressure to quickly generalize between tasks. This work argues that these two streams of hand control, namely “fractionated” and “synergistic” control, may interact to produce versatility, and balancing these subsystems may be a key part of the optimization function when learning new skills^{21–23}. This dualism is likely not rigidly dichotomous, but rather a spectrum of overriding fractionation (so-called “New M1”) atop a phylogenetically older system of synergistic action²⁴. Griffin and colleagues found that CM cells are functionally tuned to a muscle’s mode of activity (agonist, antagonist, fixator) to “bypass spinal cord mechanisms and sculpt novel patterns of motor output that are essential for highly skilled movements”²². The hypothesis stemming from the previously described work is that CM connections override the “consolidated” patterns putatively generated via spinal interneuron circuitry. The setup devised in our work aims to measure fractionation by tracing motor unit correlations across learning. Whether fractionation in our experiments is due to the CM pathway can only be speculation, but our work may provide direction for future studies pairing intracortical recordings with careful electromyography.

2.4 Supraspinal Motor Maps

It is known from recent work that primary motor cortex (M1) is not an isolated movement-generating dynamical system, but rather a node in the network of a feedback-modulated, distributed movement machine⁴. Thinking of the structural architecture of M1 as an input-driven system with outputs along a spectrum of modularity from synergistic to fractionated, we can ask what kind of functional architecture might have evolved in the neuromuscular controller? Graziano and colleagues found that 500ms electrical stimulation to M1 reliably produced stereotyped movements in primates²⁵. These movements appeared to produce goal-oriented actions pulled out of other contexts such as bringing food to the mouth, and seemed to be arranged on the cortical sheet topographically in terms of spatial endpoints rather than as a humunculus. Graziano refers to this as the cortical “action map”, that these stimulations tapped into the control mechanisms of the primate’s motor system²⁶. These results have recently been confirmed by optogenetics work in marmosets and macaques.^{27,28}

The motor map concept suggests interpreting activity in M1 as a field of feedback control microcircuits, integrating and transforming inputs, both internal and external, to sculpt ongoing movement²⁹. This is in accordance with the idea that there is a structural hierarchy in M1 covering a spectrum of movement modularity. These ideas together form a picture of the motor system as a structural scaffold upon which behaviorally relevant feedback mappings from cortex to the spinal cord are continuously activated and modulated based on information and estimates about the periphery. In this view, the encoded variables of interest depend on the goals, context, and perturbations of the intended movement. Fig. 2 shows Graziano et al.’s stimulation results, what might be termed a functional view of the cortical motor system, next Strick et al.’s described above clarifying the structural view of modularity in this system.

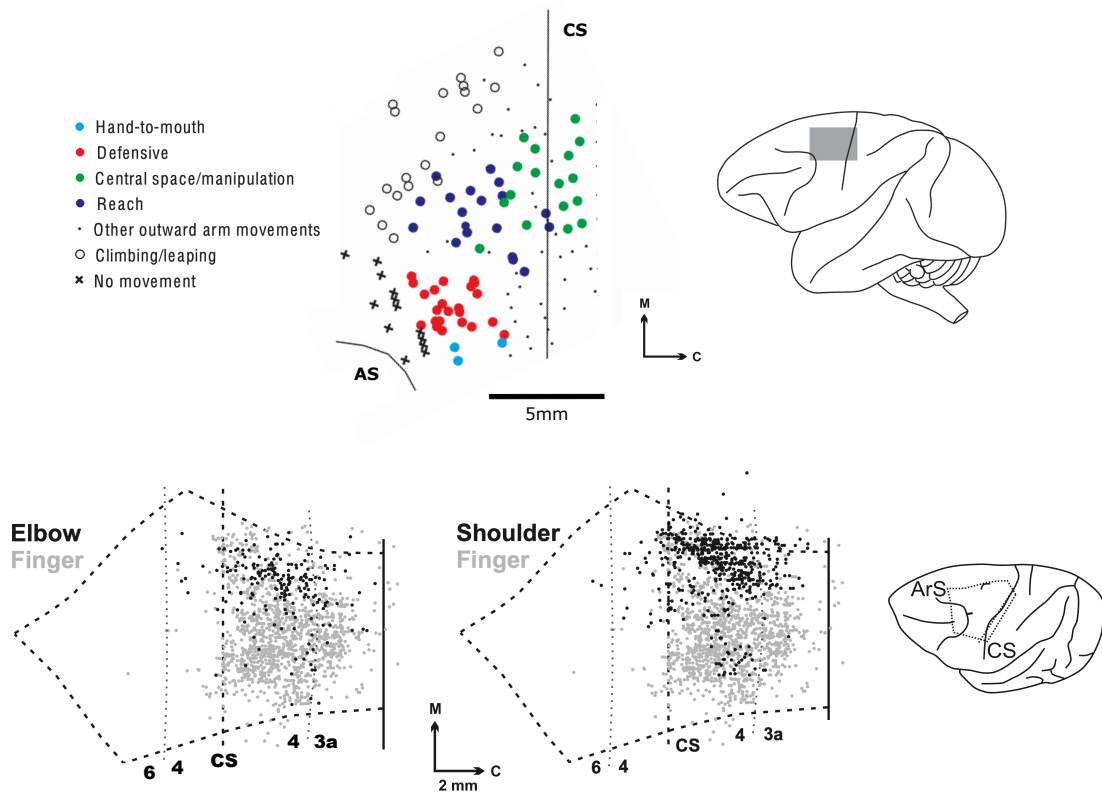


Figure 2: Similarities between electrical stimulation on behavioral timescales and rabies tracing identification of CM cells. CM cells are largely confined to the caudal half of M1, while this region tends to evoke complex manipulatory movements when electrically stimulated. (Top Left) Corticomotoneuronal (CM) cells traced using rabies from muscles of the elbow and finger. (Top Right) CM cells traced using rabies from muscles of the shoulder and finger. (Bottom) Complex movements evoked by 500ms electrical stimulation pulse trains. Adapted from Graziano 2005 and Rathelot et al. 2009^{21,30}.

Graziano writes:

"The usefulness of a feedback-dependent mapping from cortex to muscles is that it can in principle allow neurons in motor cortex to control a diversity of movement variables, such as direction, speed, hand position, or posture that transcend a fixed pattern of muscle activation. If the network receives feedback information about a specific movement variable, then it can learn to control that variable."

Muscle activity is, in this sense, a readout from a network transforming state-dependent inputs into movement goals. Rather than choosing muscle patterns in reconfigurable blocks, it creatively constructs and sculpts movement. The hierarchy of the motor system may not be rigidly organized around a particular set of variables. As shown in Fig. 3, many loops exist connecting cortex with the spinal cord, the cerebellum, the basal ganglia, and the sensorimotor periphery. Each of these loops contributes information for the flexible activation of the relevant action maps. Put simply, prevailing evidence suggests that cerebellar loops provide predictive state information while basal ganglia loops provide state and/or action value information. Taken together, this work provides an image of the incredible complexity which generates dexterous movements of the hand. This is the foundation on which we can work to build experiments which elucidate the computations involved in the production of skilled movement. We aim to connect our results back to what is known about the system we are attempting to reverse-engineer in order to inspire future inquiries into the inner workings of the movement machine.

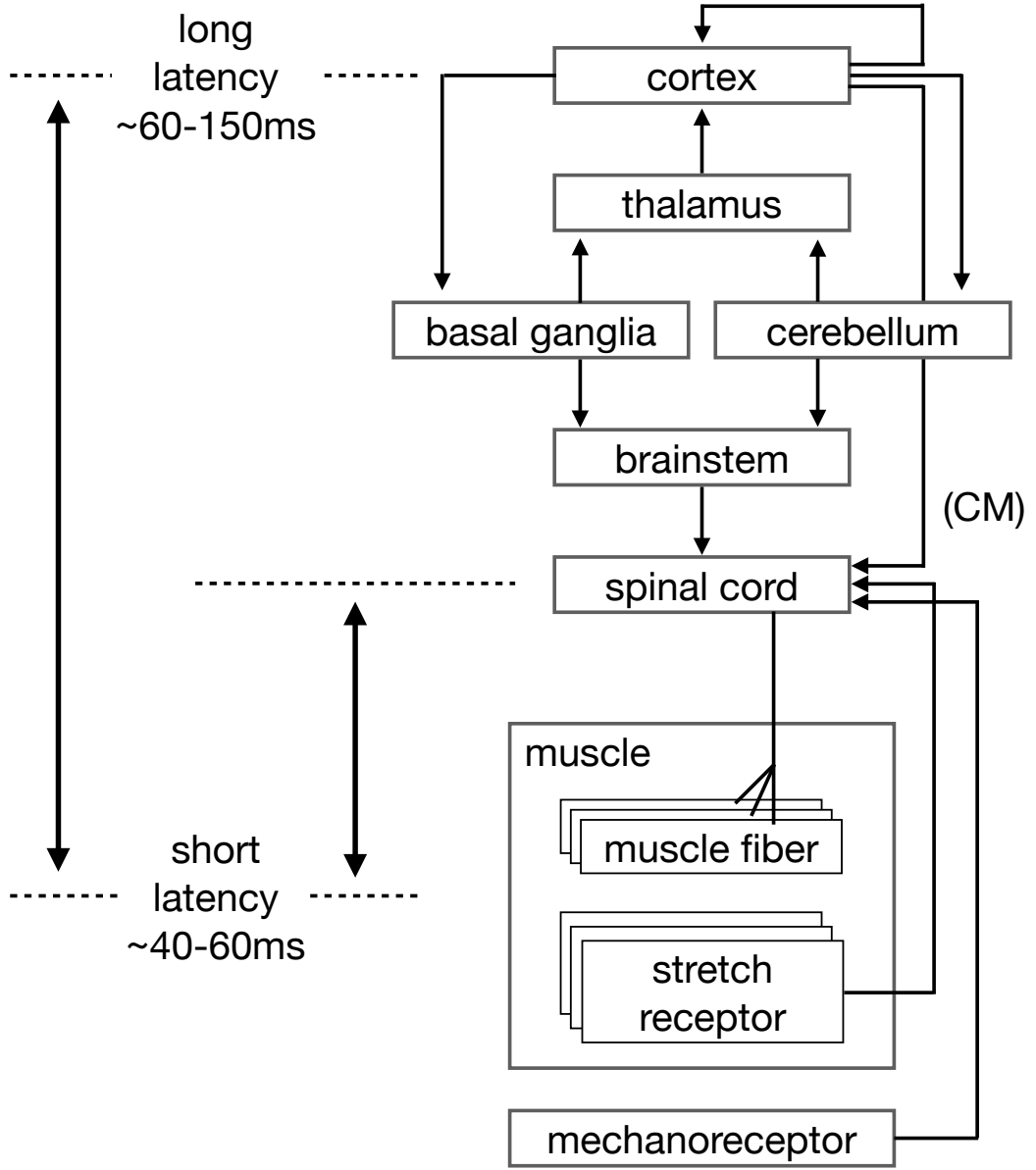


Figure 3: Overview sketch of the motor system depicting the the redundancy of the system both hierarchically (multiple muscle fibers are innervated by the same motor neuron, many motor neurons innervate the same muscle) as well as heterarchically (parallel spinal, corticomotoneuronal, cerebellum, basal gangliar feedback loops). Parallel reflex responses can be classified as long latency (approximately 60-150ms) and short latency (approximately 60ms). We hope to consider the parallelism and redundancy of the motor system to inspire our data analyses and models of motor computation.

3 Preliminary Experiments

We have some idea as to the intricate design of the puppet and the puppet strings, but we lack insight into the mind of the puppeteer.

— Bizzi & Ajemian, 2020

3.1 Recording Setup

The concept of the experimental setup is shown in Fig. 4, where 32 monopolar electrodes are attached to a subject’s forearm to record muscle activity. The arm and hand are kinematically constrained in a custom fixture and motor activity is recorded during low-level isometric muscle contractions. The setup circumvents the limb biomechanics by mapping muscle output directly to virtual stimuli shown on a screen. By focusing on low-force, isometric contractions we intend to avoid complications due to artifacts in dynamic, high-force movements.

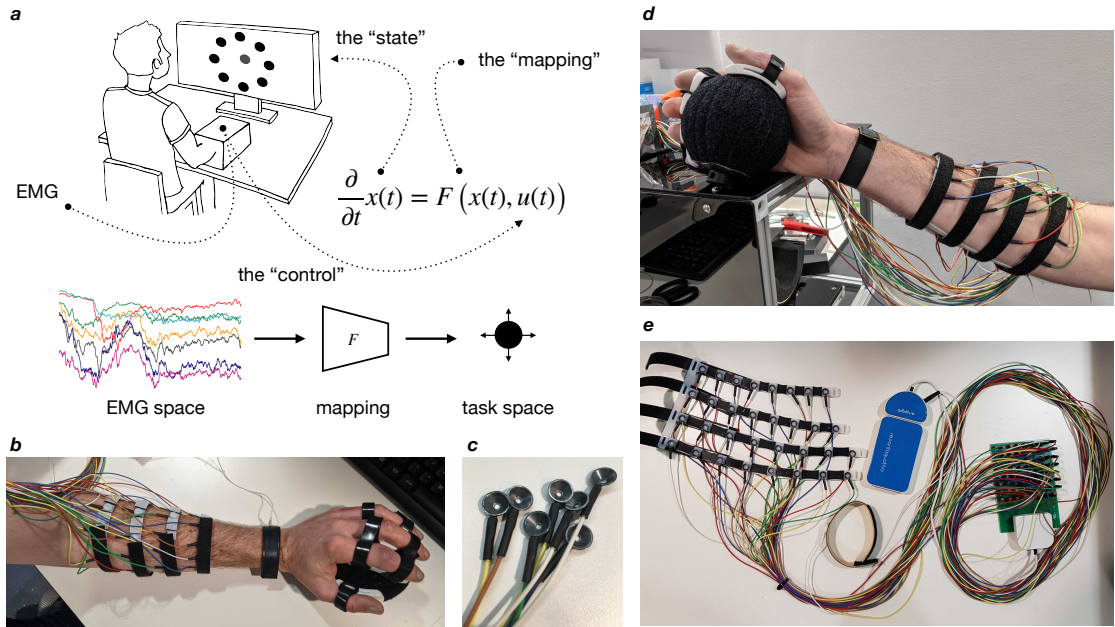


Figure 4: (a) Graphic depicting the closed-loop EMG interface concept in a center-hold, reach-out type task. The multidimensional EMG signal is transformed online through a mapping F from EMG electrode space to a lower dimensional task space. In experiments shown here the task space is a two-dimensional, though the EMG interface can be extended to tasks with higher-dimensional inputs. The subject’s arm and hand are constrained during the experiment to ensure isometric contractions. (b) First prototype of custom recording hardware consisting of four bands of eight electrodes each, and a spherical hand constraint. Our recordings are 32 channel monopolar recording with reference electrode at the wrist. (c) Example cup-style monopolar recording electrodes, 5mm in diameter. (d) Side view of the recording hardware. Also pictured is the arm restraint frame to ensure isometric contractions. The frame obscures the subject’s arm from view and contains adjustable elbow and wrist rests. (d) Recording hardware shown off the arm with wireless amplifier and connection board.

As far as we are aware, this setup is novel in combining a high number of channels with an abstract mapping. Learning experiments have used joint angles and a few muscles (typically movements of the wrist or pairs of thumb and intrinsic hand muscles), but none have taken a data-driven approach in constructing a virtual learning environment in the style of cortical BMI^{31–34}. Our EMG recording setup is custom-built: the “Sessantaquattro” EMG amplifier was acquired from OT Biolettronica, the electronic connector was designed in-house, the electrodes were acquired from Medkit UK, and the recording software was written in a mixture of Bonsai (C#) and Python.

EMG is acquired at 2kHz sample rate with 24-bit precision. A clip of raw data is shown in Fig. 5.

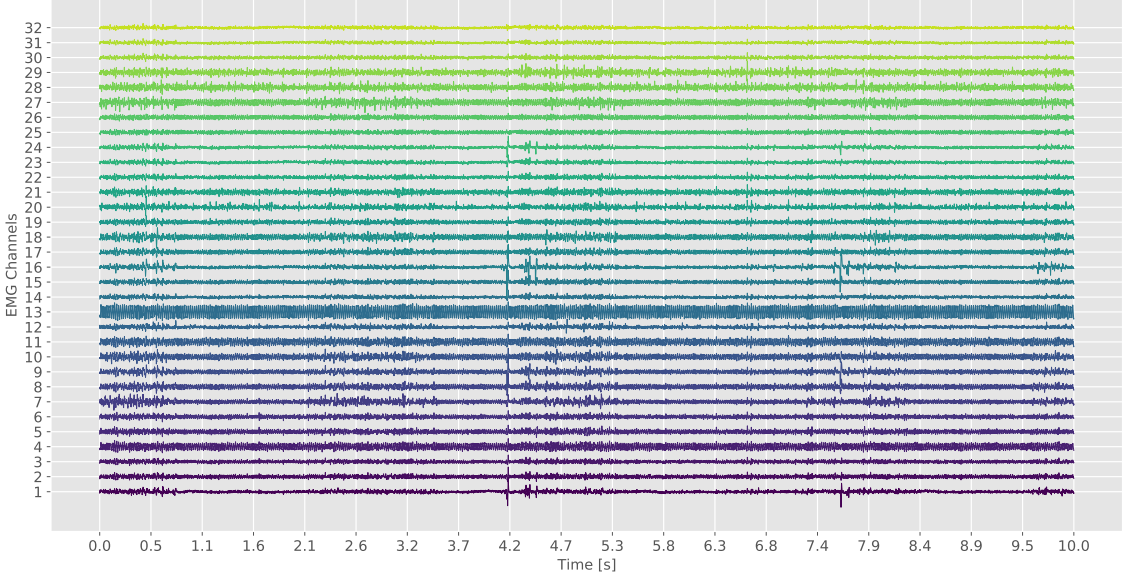


Figure 5: 10 seconds of raw 32-channel EMG data taken during a minimal finger flexion trial. Note that some channels include a nontrivial amount of line noise. This noise will be drastically reduced through changes being made in the next recording hardware revision which include shielding, shorter cables, and better cable routing. Note that some channels (e.g. channel 24) show very low noise and putative single motor unit action potentials can be seen on many channels.

To preprocessing the data, simple filtering and rectifying were applied, as is commonly done in the literature^{35–38}. As shown in Fig. 6, here we apply highpass filtering at 40Hz to remove any low-frequency oscillations and DC offsets, rectification and lowpass filtering at 5Hz to extract what is typically associated with a force readout of the EMG signal in the case that electrodes are positioned over the belly of a single muscle. These filter parameters were chosen by visual comparison across a range of values. While these preprocessing steps are in accordance with the literature and yield a signal with frequencies on a behavioral timescale though, as discussed in Section 5, preprocessing of raw EMG signals is an area worth investigating the development and application of more advanced methods.

3.2 Open-loop Finger Recordings

In our first preliminary experiment, a single subject produced flexions and extensions of each finger in the recording setup without any kind of artificial feedback. One trial was collected per finger movement in three blocks per session and one session per day over five days for a total of fifteen trials per finger movement. The purpose of this experiment is to determine the robustness over trials and sessions of EMG features for a simple low-contraction movement, as well as to determine the level of noise and artifacts in the data. Such baseline measurements are important to properly decompose variability due to electrode placement and exogenous noise from behavioral and physiological variability in order to ensure reproducibility of our results. Additionally, this baseline task may prove useful as a benchmark for later tasks in terms of testing analysis and decomposition techniques. A plot of all 32 channels for a single trial after preprocessing is shown in Fig. 7.

We first asked whether PCA applied to each individual trial would extract a single, high-variance component reflecting the dimensionality of the behavior. Since each finger movement is intuitively one dimensional, we predict that PCA would find a single high-variance component when run on each individual trial. As shown in Fig. 8, this is generally the case, though there are some outlier trials. After inspecting these outlier trials, it is likely that the subject moved multiple fingers in these trials counter to the experimenter’s instruction.

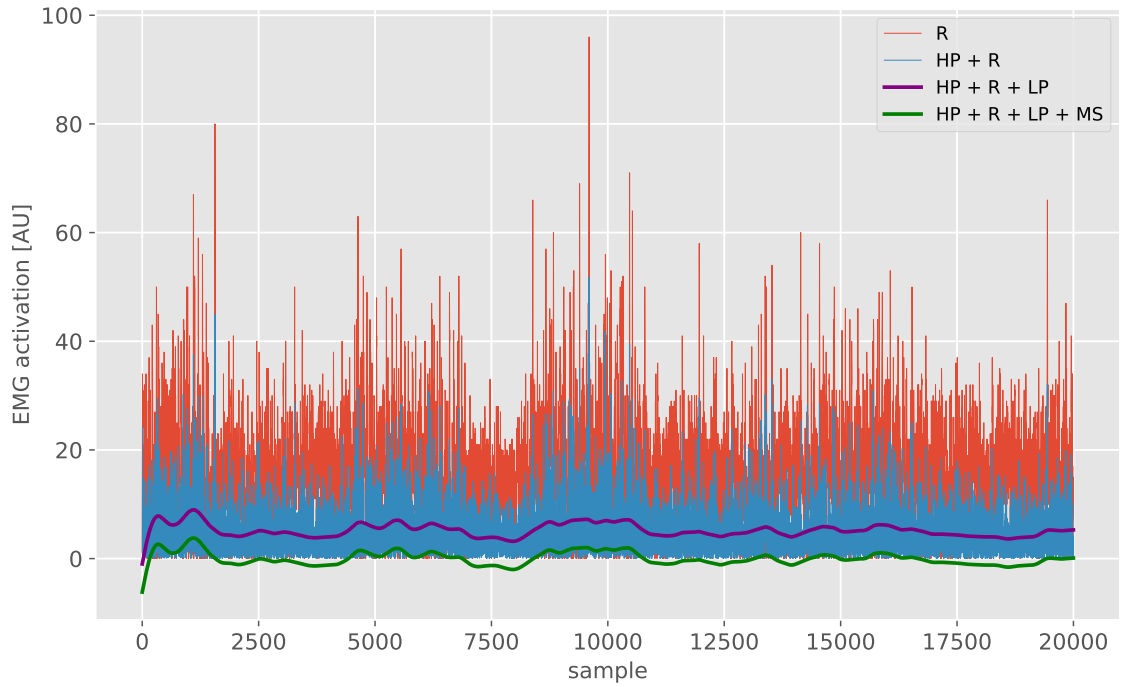


Figure 6: Data from a single trial showing each step of preprocessing. The prototype preprocessing pipeline is highpass at 50Hz, rectification, and lowpass at 5Hz. The within-trial, per-channel means are subtracted from each trial. This matches what is typically done in the literature to find a correlate of intended force^{35–38}. There is significant room for improvement on this workflow, as discussed in the text.

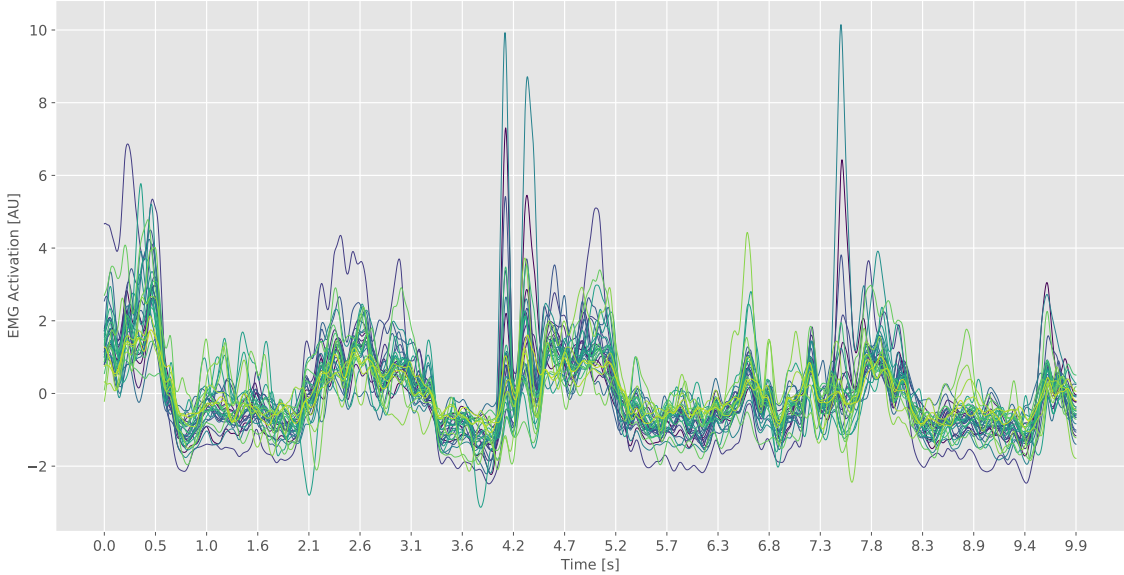


Figure 7: All channels of data from a single trial after preprocessing. Note the difference in baseline for each channel. Ideally, each channel has a clear baseline of no activity, as further discussed in the main text.

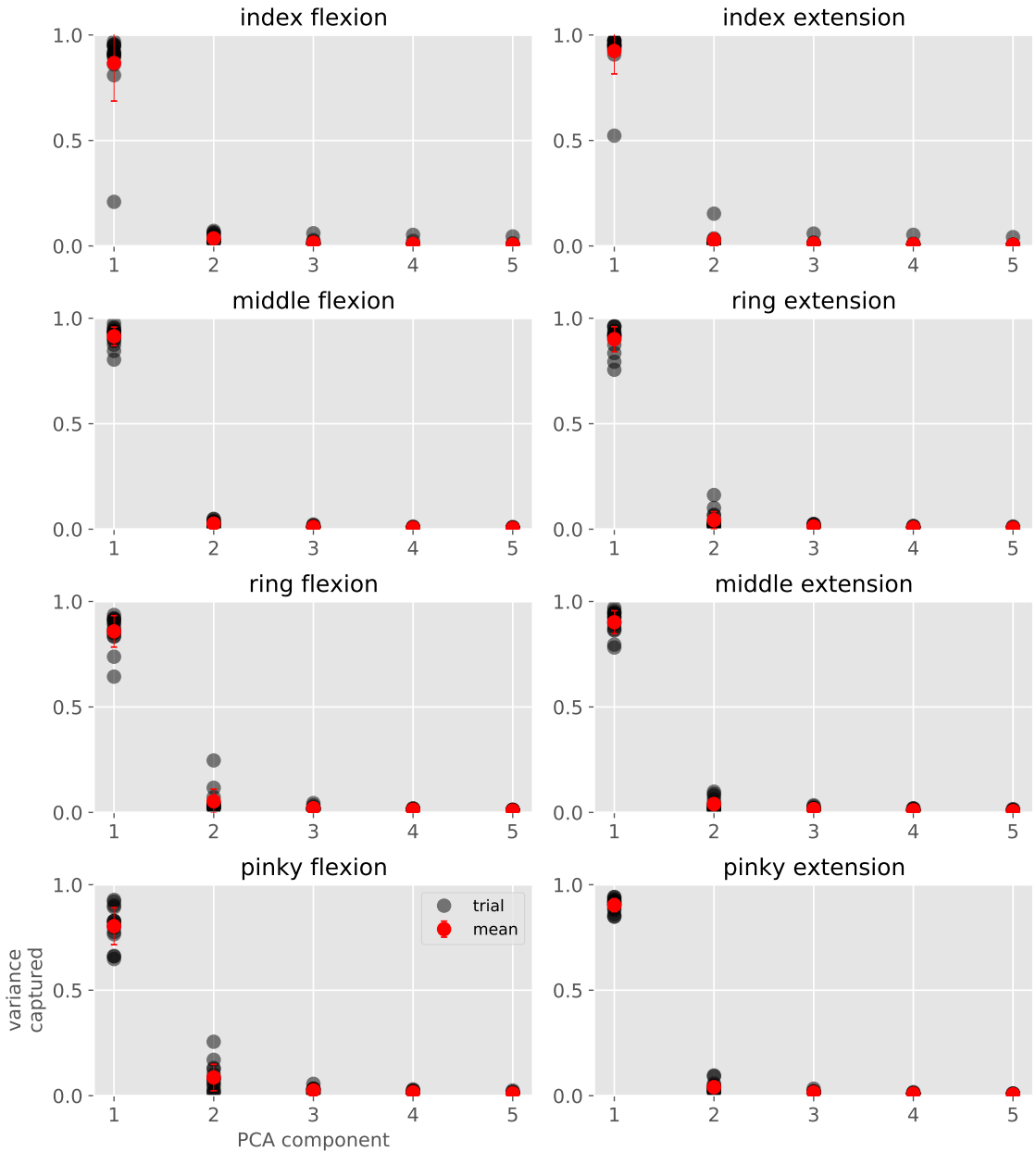


Figure 8: Fraction of variance captured by the top 5 principle components for trials of single finger extensions and flexions. PCs were computed for individual trials. Trials were recorded from one subject for 10s each trial with finger movement frequency approximately 1Hz. Three blocks each with one trial per finger movement were recorded per day for 5 days for a total of 15 trials per finger. Electrodes were not removed between blocks but were removed between days. Each trial displays a single high-variance PC component.

We next asked, since each trial appeared to be dominated by a single principle component, whether this top component was stable across trials and across days. If the top component is stable, it implies that the recording apparatus is robust to electrode movement between sessions. The top components for each movement after running PCA on each trial are shown in Fig. 9. While it is not typical to run PCA on individual trials, for the purpose of visually inspecting the PCA weights over EMG channels it is used here.

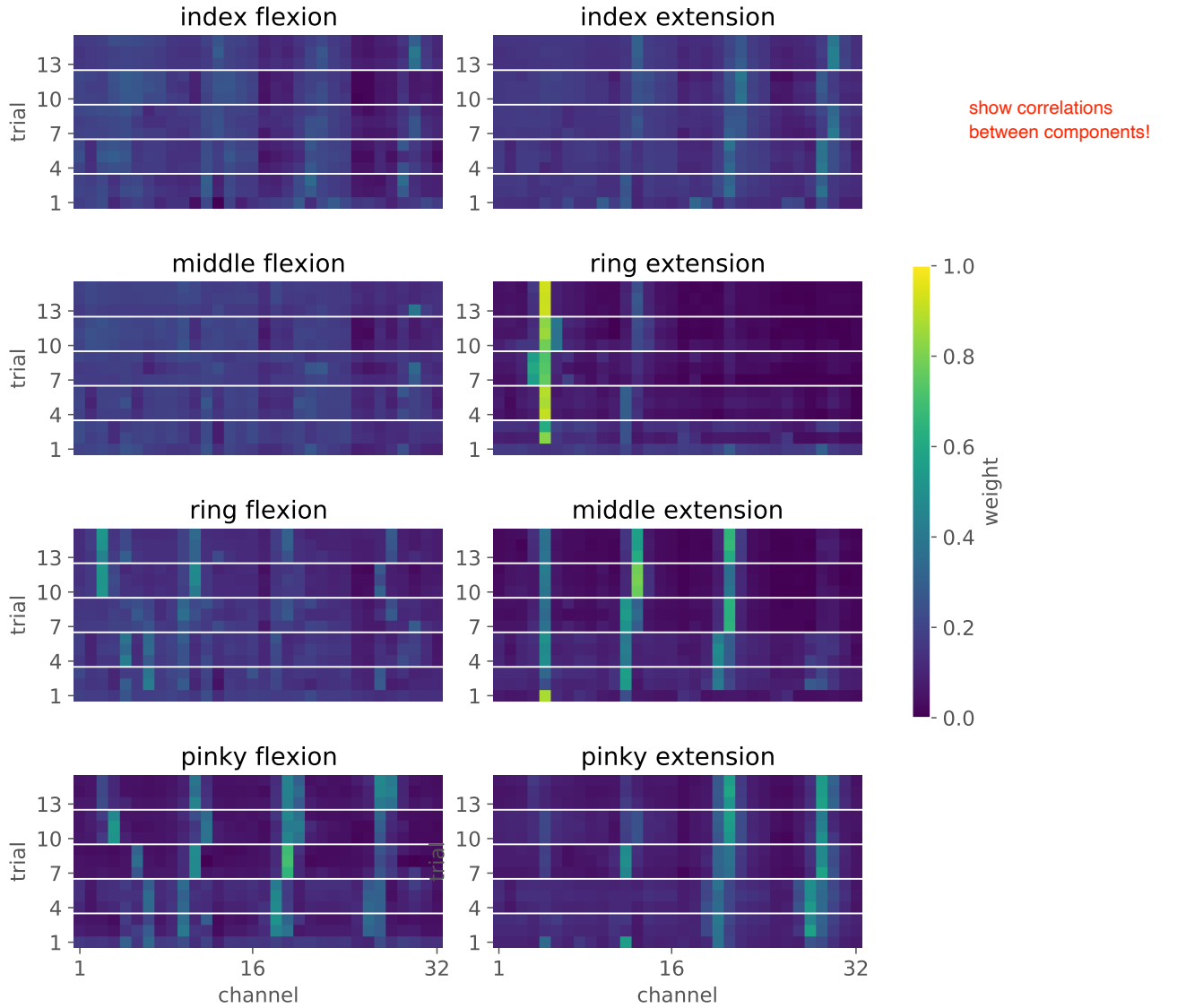


Figure 9: The top principle component from each single finger movement trials plotted as weights across channels. PCA was computed for each trial individually. White horizontal lines show breaks between days when electrodes were removed and reapplied. Each trial's top component is relatively stable across trials and across days, though there is drift and dropout of weights. Measures to increase cross-session stability are discussed in the main text. Movements appear to vary between strong localization on single channels and broad activation across channels.

The results here suggest that, at least up to linear decompositions, the features of low-contraction movements is relatively robust across sessions. As discussed in Section 5, we will construct more reliable means to place electrodes on subjects' forearms to further increase repeatability. Another aspect of these results is our assumption subjects are producing the same contraction each time they move their finger, and at the same contraction level. That is, we assume they are recruiting

the same motor units each movement. This may not be the case, and constructing new analyses which infer motor unit activations may be useful to mitigate this issue.

3.3 Center-hold Reach-out Task

In this task, the 32-dimensional EMG electrode activity vector is mapped to a 2D force acting on a point mass shown on the screen. The mapping $M \in \mathbb{R}^{2 \times 32}$ maps 8 “columns” each consisting of 4 electrodes placed in a line down the length of the forearm each to one of 2D root of unity. Each column of electrodes is thus mapped to one of 8 two-dimensional force vectors. In this experiment, the point mass has zero inertia and zero friction and as such displays a direct, though redundant, readout of the EMG signal. The task asks the subject to reach one of 32 equally spaced targets on each trial. Subjects must hold in the center of the task space for a designated period of time, after which the target appears. Subjects then have a time window reach the target. Data from one subject was recorded for three blocks in one session. Each block consisted of 32 trials, one per target in a randomized order.

The mapping between EMG and task space M can be written as

$$M = [\tilde{M} \quad \tilde{M} \quad \tilde{M} \quad \tilde{M}]$$

where \tilde{M} consists of 8 equally spaced directions, one for each “column” of the 4 EMG electrode bands around the subject’s arm:

$$\tilde{M} = \begin{bmatrix} 0 & 0.71 & 1 & 0.71 & 0 & -0.71 & -1 & -0.71 \\ 1 & 0.71 & 0 & -0.71 & 1 & -0.71 & 0 & 0.71 \end{bmatrix}$$

A graphic showing the mappings from electrodes to force directions is shown in Fig. 10. While there are 8 possible force vectors the subject can modulate by controlling the electrode activity on each of her 8 columns, the EMG mapping is ultimately a projection onto the 2D plane. Since the EMG signal is nonnegative, the subject could technically modulate just four modes of electrode activity, the minimum number needed to span the task space, to reach all 32 targets. This mapping was chosen in order to provide a simple starting point to explore the virtual EMG task. There are no added environmental dynamics, only a redundant readout of force, and the signal is processed online in the same manner as in the offline analyses. This task or a variant we think can serve as a foundation upon which we can build more complex mappings and virtual environments. Task space trajectories from each block are shown in Fig. 11. The fraction of trials resulting in hold timeouts, reach timeouts, and target hits are shown over blocks in Fig. 12.

In this task, the subject’s first goal is to interact through the mapping M and learn the consequences of various motor activations. That is, they must internalize a model of the virtual environment, what might be called a system identification problem. Subjects must collect data containing motor outputs and their sensory consequences. To do this, they must explore the space of activity. We predict that over trials, subjects’ EMG activities over channels will become more varied as they attempt new movement patterns to achieve their twin goals of learning to move in this new environment and reaching the target. Running PCA on each individual trial’s EMG time series, we hypothesize that initially we will see multiple components share signal variance as subjects explore. Eventually, we would expect to see a decrease in this measure of movement complexity as subjects hone their reaching skill. Trial-level PCA component variance fractions are shown in Fig. 13. We find an initial decrease in the top component’s variance fraction, though we expect many more trials will be needed to see skill acquisition in the form of a dominant movement mode per trial.

We might model this task as the subject selecting an EMG signal x which minimizes the distance between a target position b and the projection of the EMG signal through the mapping M as well as minimizes the norm of x in order to conserve metabolic energy. This optimization can be written as a regularized least squares problem:

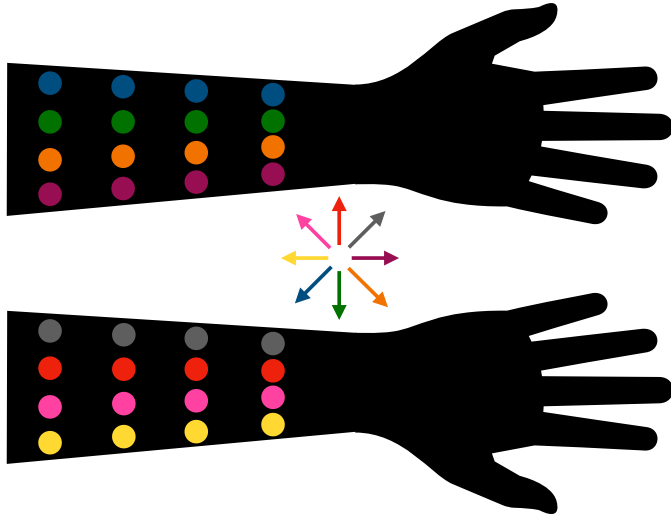


Figure 10: Graphic showing the mapping between electrodes in the 32-channel center-hold reach-out experiment to eight 2D force directions in the virtual task space. Each of the eight columns consists of four electrodes each mapped to the same force direction (denoted with matching color) acting on a virtual point particle.

$$\min_x \frac{1}{2} \|Mx - b\|_2^2 + \frac{\lambda}{2} \|x\|_2^2.$$

This problem is known to have a unique minimum for $\lambda > 0$ which is an approximation $Mx \approx b$ regardless of the shape or rank of M . This implies that the subject, if they are biophysically capable to do so, will learn distinct motor outputs for each target rather than reusing modes for multiple targets with different activation levels. That is the subject will, over time, learn to fractionate their muscle output to reach their goal in order to minimize effort. For instance, to reach the target at position $(1, 0)$ in Cartesian coordinates, the subject could activate a bespoke activity mode and activate a combination of two or more modes for targets at $\pm 45^\circ$ from this central target. If this is the case, the model predicts that the dimensionality of the EMG signal will increase over the course of training as the subject learns to construct bespoke activity modes for each target.

In Fig. 14 we compute PCA on the concatenation of all trials within blocks for which we predict an increase in the number of dominant EMG modes as subjects learn multiple movements to reach individual targets. We expect subjects to, over time, develop some number of bespoke movement modes to activate independently and as a composition to reach each target. We find a suggestion of this idea in the data with our basic PCA analysis. More trials, session, and subjects will be required to explore this idea, and we are investigating probabilistic measures of signal complexity such as entropy to formalize this hypothesis. One direction might be to further define this task a regularized regression with different regularization terms chosen normatively for different sections of the learning and control process, and fitting data to these predictions. For instance, early in training subjects may not optimize for target accuracy as much as for signal sparsity, whereas later in learning subjects may optimize for target accuracy and output signal magnitude.

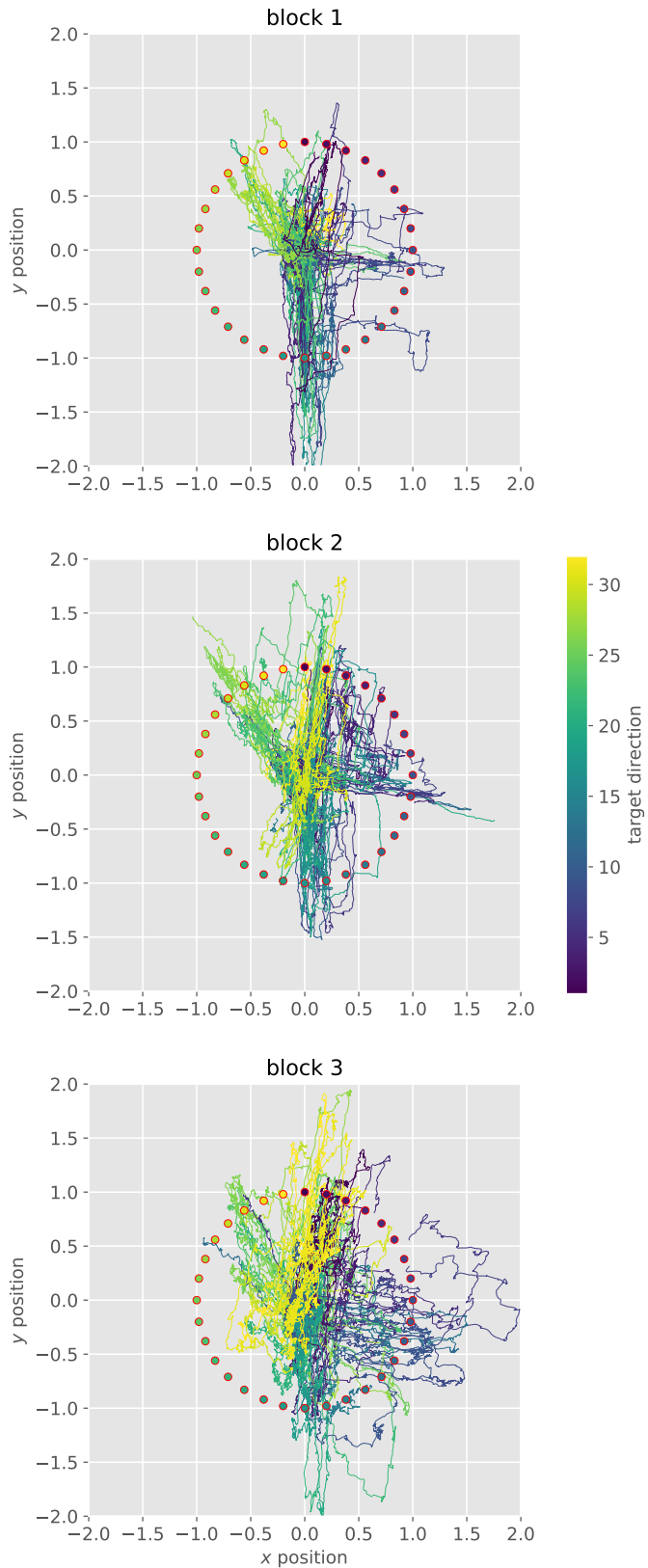


Figure 11: Point mass position trajectories in two-dimensional task space during the center-hold, reach-out task with 32 targets spaced evenly around the unit circle (shown with red borders). Color corresponds to target numbers, with target zero located at $(0,1)$. Target order was randomized. Training was conducted over 3 blocks each with 32 trials, 1 trial per target.

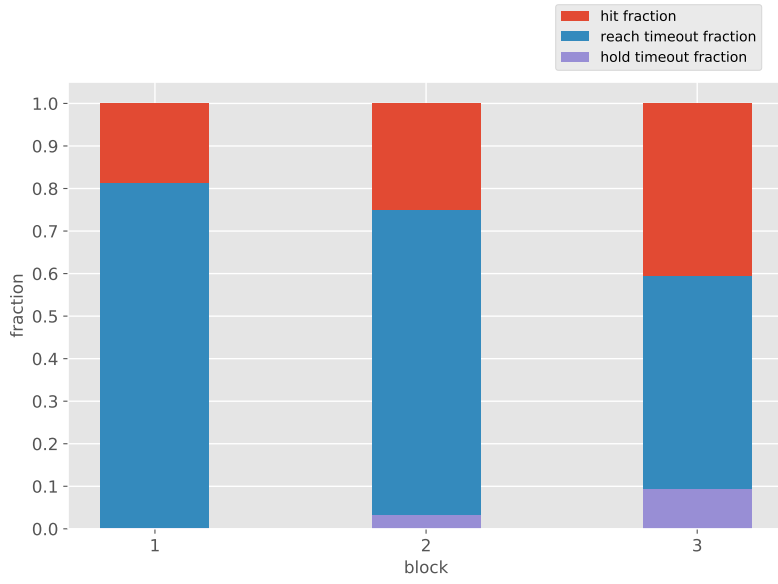


Figure 12: Fractions of trial outcome types for each block of the center-hold, reach-out task. Hit fraction increases on each trial, suggesting the beginnings of task learning. Hold timeout failure increases over trials as well, perhaps suggesting increased baseline excitation of muscles during the hold period. Part of learning to activate certain muscle modes is learning to inhibit others.

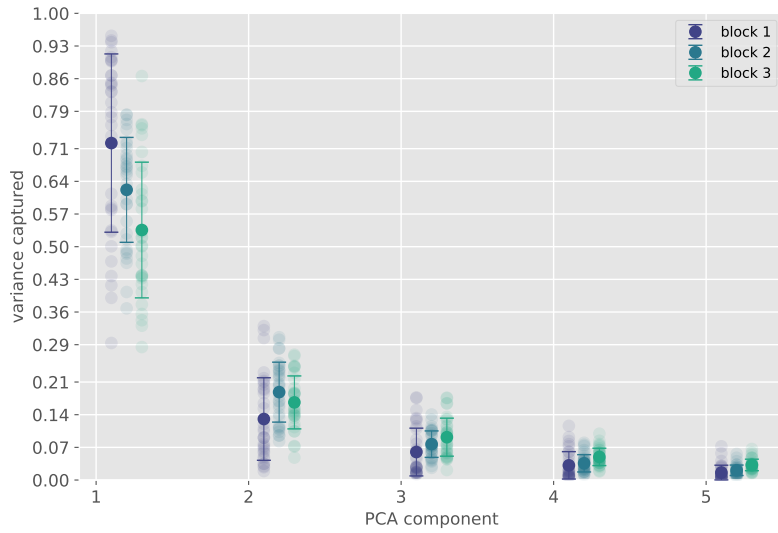


Figure 13: Fraction of variance captured by the top five principle components when PCA is run on the EMG time series' of individual trials of the center-hold, reach-out task. Error bars are standard deviation. Over blocks, we see a slight decrease in the mean of the top component's variance fraction, though with high variance. This may suggest greater exploration within-trial, as less variance is captured by a single component over blocks, though it could reflect more varied dynamics across trials as the subject discovers new, task-relevant activations.

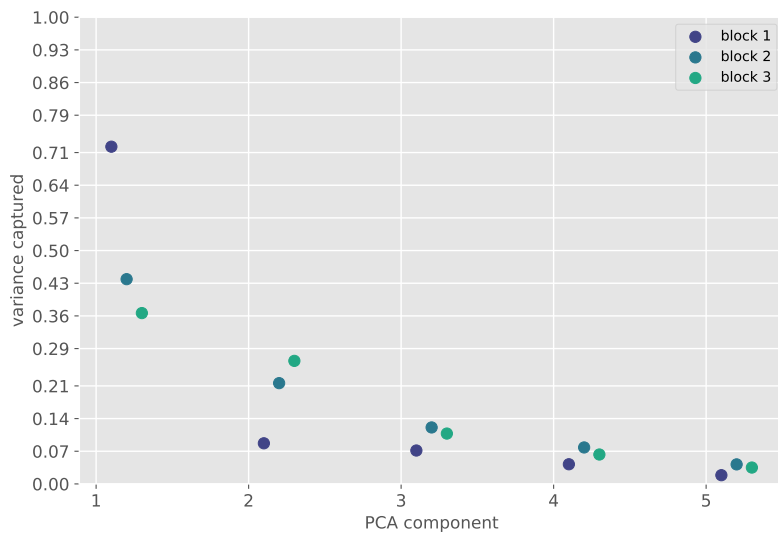


Figure 14: Fraction of variance captured by PCA computed on concatenated EMG time series concatenated over trials. Over blocks, we see variance shifting from the top component to other components. We hypothesize that across learning we would see the development of bespoke modes used in combination to reach individual targets. This would predict an increase in the complexity of the EMG time series over learning. Here we see suggestions of this prediction.

4 Preliminary Theory

An interesting open question is how to relate trial-to-trial dynamics of learning to asymptotic predictions regarding optimal adaptation.

— Todorov, 2007

4.1 Optimal Feedback Control

The optimal feedback control framework remains the strongest normative model of human movement control. The first step of our theoretical work is to build from the simplest optimal feedback control models, working towards constructing our own variants of such models in order to capture aspects of our experimental findings. The first model we will investigate is the fully-observable, discrete-time, infinite-horizon linear quadratic regulator (LQR) problem with additive Gaussian noise. Given a state $x \in \mathbb{R}^n$ and a control input $u \in \mathbb{R}^m$, the state evolves in discrete time according linear dynamics

$$x_{t+1} = Ax_t + Bu_t + w_t$$

where $w_t \sim \mathcal{N}(0, \mathbb{I})$. The LQR problem is to find a sequence of controls u_t which minimize a cost J

$$J = \mathbb{E} \sum_{t=0}^{\infty} x_t^T Q x_t + u_t^T R u_t$$

according to some chosen state and control cost parameters Q and R . The optimal cost-to-go or state value function for the problem is

$$V_t(x) = \min_u [x_t^T Q x_t + u_t^T R u_t + V_{t+1}(Ax + Bu)].$$

The optimal control law L which solves this problem is linear function in the state

$$u_t^*(x) = -Lx.$$

This control law is found through iterating a Riccati equation involving A , B , Q , and R to find the optimal V which is a quadratic function in state. There is a functional relationship between V and L that can be derived algebraically. Fig. 15 shows simulated trajectories of the infinite-horizon problem from random initial positions. The vector field depicts the two-dimensional control vector. In this example, the model describes a second-order point mass dynamical system where the control input acts as a force on the particle. The state vector x contains two dimensions each of position, velocity, and force of the particle, each updated via Euler integration. Fig. 16 shows the same simulated trajectories of the point mass atop the quadratic value function. The goal state in these simulations is $(0.5, 0.5)$. Note that there are many free dynamics parameters in such simulations within A and B which drastically alter the resulting simulations. The values here were chosen to match the motor control literature.

Assuming that the original system is controllable and stabilizable, the linear optimal control problem is a matter of trading off eigenvalues of the closed loop system which drive the steady-state error of the system to 0 under the control cost. This system can be made to drive to a given target x^* by feeding back evolving the dynamics in terms of target error $|x - x^*|$ or by augmenting the state vector with terms which compute this error implicitly. These yield identical solutions for the control law, the latter typically being more convenient. The implication of this is that only one control law is required for the problem with a point target in the state space. If the problem were to model human movement, it might be said that we only require the internalization of a single control law up to a translation in the target's desired state. Only the error is required in this simple case. As discussed in Section 5, variants of this basic model are more interesting in that they do not display this target invariance.

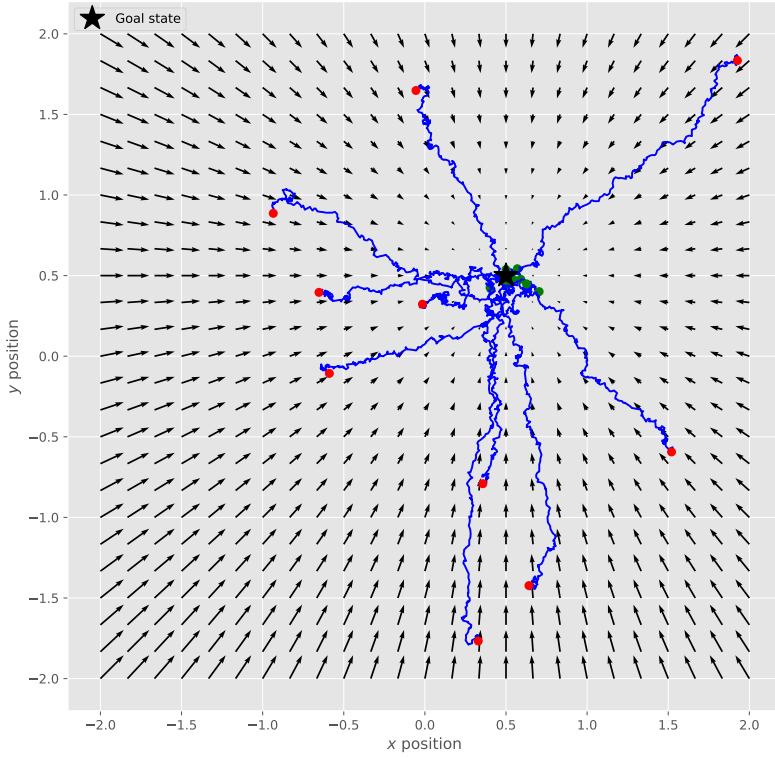


Figure 15: Simulation of trajectories from uniform random initial positions for the simplest LQR controller. The diffusions are controlled such that their inputs are proportional to the positional error. The plain LQR controller is invariant (up to a translation) to the goal state, as explained in the text. Here the goal state is $(0.5, 0.5)$ denoted by a white star. red circles denote the initial position of the trajectory and green circles denote the endpoint after 200 increments. Arrows show the state-dependent control signal (force) vector $u^T = [f_x, f_y]$.

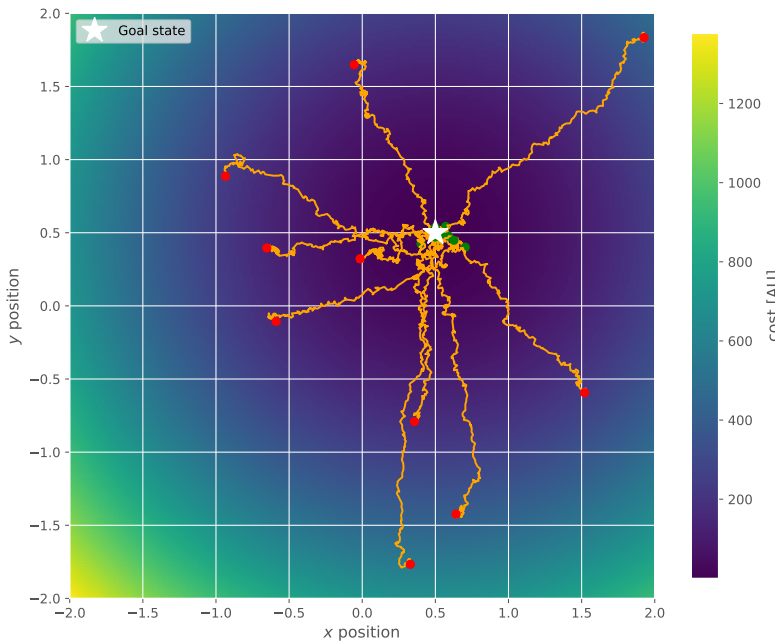


Figure 16: The same trajectory simulations as in Fig. 15 atop the quadratic cost field.

4.2 Internal Model Adaptation for Linear Quadratic Control

In experiments within the setup described in Section 3, subjects are faced with a novel muscle-to-environment mapping that they must ostensibly learn in order to achieve their goals. Here I investigate the effects of approximating dynamics models within the LQR framework. This short experiment is a first step in modeling how subjects may use endpoint error in each trial to update or adjust their internal approximations of the environment’s dynamics.

Our state space is denoted x and our control space u where $\dim(x) < \dim(u)$. Each trial, we move from state x_0 to $x(N)$ in N timesteps. Each trial, we have a goal state x^* and a resulting endpoint error $e_N = |x_N - x^*|^2$. We follow the same LQR setup as defined in the previous section. We can write the controlled, closed-loop system dynamics for the final time step N :

$$\begin{aligned} x_N &= (A - BL)x_{N-1} = Cx_{N-1} \\ x_N &= Cx_{N-1} = C(Cx_{N-2}) \\ x_N &= C^N x_0. \end{aligned}$$

where C^N might be called the trajectory dynamic. If the trajectory dynamic C^N is an approximation to the true trajectory dynamic C^{N*} , we can use the error of a given trajectory to find an incremental update. The error at the final time step N for trial r is

$$e(r) = |C^N(r)x_0 - x^*|^2.$$

This error may be due to several sources. Our internal dynamics model A might have error relative to the true dynamic A^* . Our control gain L may be optimal relative to our internal model A but not with respect to the true dynamic A^* . Finally, we might have an approximate model A and a suboptimal control gain L . Note that since this is still deterministic system, we have yet to include any source of variability in state or control.

If we assume that our computation of the control gain L is optimal for our approximate internal model A (we can compute a controller given only our internal representation of the system dynamic being controlled), we can use our endpoint error to derive a gradient descent update for A on trial r :

$$A(r+1) = A(r) - \eta \frac{\partial e(r)}{\partial A}$$

We might think about this as an internal simulation of trial r ’s trajectory, and a subsequent post hoc evaluation of the movement. To compute δ , we must take the gradient with respect to A of the error:

$$\frac{\partial e(r)}{\partial A} = \frac{\partial}{\partial A} |C^N(r)x_0 - x^*|^2$$

Since the gradient with respect to A is the same as the gradient with respect to C , we can compute the gradient with respect to C to find:

$$\frac{\partial e}{\partial A_{ij}} = 2 \sum_{k=1}^N [(C^N x_0 - x^*)^T C^{k-1}]_i [C^{N-k} x_0]_j$$

Fig. 17 shows the LQR simulations across gradient descent updates to the A matrix after it is corrupted by Gaussian noise. Each trajectory is a single run of the LQR controlled for 200 time steps. The star shows the target state, the colored circles show the endpoints of the trajectories. The red circle is the initial state. The descent is converging in endpoint error in position, velocity, and force dimensions of the state vector. Unfortunately, this optimization alters the dynamics

incompatibly. The routine is also very fragile to parameter changes. This experiment highlights the difference in loss landscapes between the optimal control problem and the gradient descent simulated here. There are many directions for this work to proceed as discussed in Section 5.

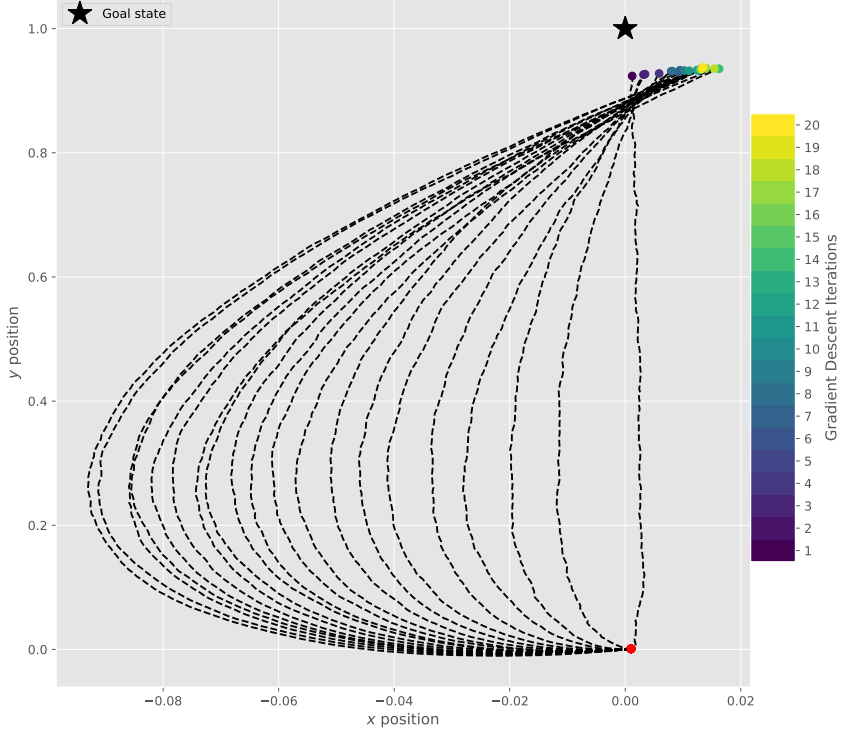


Figure 17: Iterations of gradient descent on the A matrix of an infinite-horizon LQR where the original A is corrupted with Gaussian noise. Each dotted line is a sampled trajectory using a recomputed control gain with an updated A matrix. Red circles denote the initial state, the star denotes the goal state, and the colored circles denote the endpoints of each trajectory sampled at each iteration. Note that the initial solution diffuses directly towards the target, and the gradient updates for the dynamics model A alter this trajectory in a nontrivial way. As discussed in the main text, the gradient descent is optimizing for a different cost than the controller optimization, and thus this divergence might be expected.

5 Next Steps

When it comes to the problem of skilled movement, the algorithm is simply not known.

— Wolpert & Ghahramani, 2000

5.1 EMG Hardware

Our preliminary data confirms the working principle of the setup and highlights the next steps for producing quality datasets. This is in accordance with the literature, where more advanced use of EMG is emerging as an important tool in understanding the complexities of motor computation³⁹. Our next steps are to build a new version of the EMG hardware doubling the number of channels to 64 electrodes placed across the forearm and to provide better hand constraints to ensure completely isometric contractions. The next hardware version will also include investments in shielding to provide proper noise mitigation. Most EMG in the literature is smoothed and trial-averaged due to noise, but we are confident that our records can be analyzed at the level of single trials, much like recent developments in neural data analyses.^{36,37}

5.1.1 Eye Tracking

To completely close the loop in our experiments, we are working to integrate pupil and gaze tracking to more closely follow the perceptual aspects of our task. We hope to find correlations in line with the literature dealing with active learning^{40,41}.

5.2 EMG Analyses

5.2.1 Preprocessing

Preprocessing of the EMG signal per-channel is another key area for improvement. EMG signal is the convolution of motor unit action potentials terminating near the electrode sites. Ideally we could filter each channel of raw EMG to infer the signal envelope. There is precedent in the literature for Bayesian filtering of EMG signal using a Laplacian distribution. Sanger used a Laplacian distribution to filter a one-dimensional EMG signal³⁵. In accordance with this choice, Nazarpour found that as more motor units are recruited, the EMG distribution shifts from super-gaussian to gaussian following the central limit theorem⁴². That work suggests methods for estimating high-order statistics for better filtering at low contraction levels relevant to our experiments. Such methods may prove to be more rigorous for inferring motor unit activations from our raw signal.

5.2.2 Calibration

With a filtered raw signal per channel, our goal is to devise mapping from EMG space to task space which are biophysically achievable by our subjects but require a degree of learning over many trials. In our preliminary task, we hardcoded mappings. Our next step would be to design a calibration task which asks subjects to actively explore the biophysical limits of EMG space that can be captured by our electrodes. This is akin to extracting features of spontaneous activity and passive viewing used in cortical BMI experiments to generate “intuitive” mappings.^{43,44}

With high-dimensional EMG, we would ideally devise a principled method of extracting modes from raw EMG that accurately reflect modes of neural drive, demixing neural modes across channels. Here we used PCA as a first step. One starting point would be to align with the cortical BMI literature and use factor analysis and Kalman filtering⁴⁴. The issue, however, is how to design a task which evokes the available modes of possible EMG activity before using dimensionality reduction to generate learnable yet non-intuitive mappings.

5.3 Task Design and Data Collection

With a working calibration task, our next goal is to use this calibration data to generate mappings to track learning. Our center-hold, reach-out task combined these two steps into one task for validation of the setup using hardcoded mappings. We can maintain the center-hold, reach-out style

of the task but with data-driven mappings, as well as construct novel tasks to test predictions of our models. Scaling this task up to multiple subjects across days will provide a dataset with which we can test hypotheses concerning the evolution of complexity and correlations across learning. This will also give us an opportunity to study inter-subject variability, for which there is precedent in the literature which suggests individual strategies⁴⁵.

5.4 Modeling Control

One relevant aspect of the basic optimal feedback control model is that the optimal controller that arises from specifying a quadratic state and control cost is invariant to the target state. In spite of this, we can use the aforementioned task to test predictions of the basic LQR model with respect to state and control noise and imperfect dynamics.

We expect to validate the basic optimal control models for our setup as we've designed the learning environment specifically for the EMG signal provided by the subject acts as the input to chosen virtual dynamics, which can be chosen in accordance with our model. We can then test perturbations in our task with respect to noise, goal, and dynamics and compare subjects' responses to our models.

The question then becomes: when might subjects need to internalize a new control policy? When might they need to internalize multiple control policies? We hope to work towards answers of these questions alongside models of compositional control. Such control models could deal with, for example, target uncertainty as well as multiple competing targets^{46,47}.

5.5 Modeling Learning

Ultimately, our goal is to adapt optimal control models which begin as coarse approximations and are updated both within and across trials. Adaptation typically refers to online alterations to control policies while learning might refer to across-trial policy changes. Our theoretical aim is to devise models of learning and movement construction which extend the optimal feedback control framework through additions of composition and error-based updates.

Stemming from our work using simple gradient descent to update internal dynamics models, we would like to gain a better understanding of the loss landscape. It may be possible to compute the optimum analytically and to corrupt the dynamics matrix in a more principled way. We will also explore the action of the resulting gradient, and compute second-order derivatives, and compute derivatives with respect to the control law K as a comparison. These results can then be compared with results from the reaching adaptation literature. This work can be guided by analyzing our empirical data to understand what aspects of our trajectories in EMG and task space are changing over trial.

5.6 Open Questions

- What is the best calibration task to find the boundaries of the available EMG space?
- What are the defining features of learning in our EMG-based task?
- Are our experiments well-modeled by the optimal control framework?
- How do subjects efficiently use error information from each trial and feedback from each time step to update their forward model and control policy/policies? How do subjects balance policy updates with model updates?
- How does a subject sample the state space to efficiently learn? Do subjects sample optimally?
- How can you empirically disentangle system identification (model estimation) and policy learning? If subjects are suboptimal, is it due to model mismatch or a suboptimal policy?

Bibliography

1. McNamee, D. & Wolpert, D. M. Internal Models in Biological Control. *Annual Review of Control, Robotics, and Autonomous Systems* **2**, 339–364 (2019).
2. Todorov, E. Optimality principles in sensorimotor control. *Nature Neuroscience* **7**, 907–915 (2004).
3. Kober, J., Bagnell, J. A. & Peters, J. Reinforcement learning in robotics: A survey. *The International Journal of Robotics Research* **32**, 1238–1274 (2013).
4. Sauerbrei, B. A. *et al.* Cortical pattern generation during dexterous movement is input-driven. *Nature* (2019) doi:10.1038/s41586-019-1869-9.
5. Bernstein, N. *The coordination and regulation of movements*. (Pergamon, 1967).
6. Kitano, H. Biological robustness. *Nature Reviews Genetics* **5**, 826–837 (2004).
7. Fuglevand, A. J. Mechanical properties and neural control of human hand motor units: Control of human hand motor units. *The Journal of Physiology* **589**, 5595–5602 (2011).
8. van Duinen, H. & Gandevia, S. C. Constraints for control of the human hand: Control of the hand. *The Journal of Physiology* **589**, 5583–5593 (2011).
9. Yan, Y., Goodman, J. M., Moore, D. D., Solla, S. A. & Bensmaia, S. J. Unexpected complexity of everyday manual behaviors. *Nature Communications* **11**, 3564 (2020).
10. Basmajian, J. V. Control and Training of Individual Motor Units. *Science* **141**, 440–441 (1963).
11. D'Avella, A., Saltiel, P. & Bizzi, E. Combinations of muscle synergies in the construction of a natural motor behavior. *Nature Neuroscience* **6**, 300–308 (2003).
12. Giszter, S. F. Motor primitivesnew data and future questions. *Current Opinion in Neurobiology* **33**, 156–165 (2015).
13. Gao, P. *et al.* *A theory of multineuronal dimensionality, dynamics and measurement*. (2017) doi:10.1101/214262.
14. Rácz, K. & Valero-Cuevas, F. J. Spatio-temporal analysis reveals active control of both task-relevant and task-irrelevant variables. *Frontiers in Computational Neuroscience* **7**, (2013).
15. Ingram, J. N. & Wolpert, D. M. The statistics of natural hand movements. *Brain* **188**, 223–236 (2009).
16. Todorov, E. & Ghahramani, Z. Analysis of the synergies underlying complex hand manipulation. in *The 26th Annual International Conference of the IEEE Engineering in Medicine and Biology Society* vol. 4 4637–4640 (IEEE, 2005).
17. Bizzi, E. & Ajemian, R. From motor planning to execution: A sensorimotor loop perspective. *Journal of Neurophysiology* **124**, 1815–1823 (2020).
18. Bruton, M. & O'Dwyer, N. Synergies in coordination: A comprehensive overview of neural, computational, and behavioral approaches. *Journal of Neurophysiology* **120**, 2761–2774 (2018).

19. Cheney, P. D. & Fetz, E. E. Functional classes of primate corticomotoneuronal cells and their relation to active force. *Journal of Neurophysiology* **44**, 773–791 (1980).
20. Griffin, D. M. & Strick, P. L. The motor cortex uses active suppression to sculpt movement. *Science Advances* **6**, eabb8395 (2020).
21. Rathelot, J.-A. & Strick, P. L. Subdivisions of primary motor cortex based on corticomotoneuronal cells. *Proceedings of the National Academy of Sciences* **106**, 918–923 (2009).
22. Griffin, D. M., Hoffman, D. S. & Strick, P. L. Corticomotoneuronal cells are "functionally tuned". *Science* **350**, 667–670 (2015).
23. Takei, T., Confais, J., Tomatsu, S., Oya, T. & Seki, K. Neural basis for hand muscle synergies in the primate spinal cord. *Proceedings of the National Academy of Sciences* **114**, 8643–8648 (2017).
24. Dum, R. P. & Strick, P. L. The Corticospinal System: A Structural Framework for the Central Control of Movement. in *Comprehensive Physiology* (John Wiley & Sons, Inc., 2011). doi:10.1002/cphy.cp120106.
25. Graziano, M. The Organization of Behavioral Repertoire in Motor Cortex. *Annual Review of Neuroscience* **29**, 105–134 (2006).
26. Graziano, M. S. A. *The intelligent movement machine: An ethological perspective on the primate motor system*. (Oxford University Press, 2009).
27. Ebina, T. *et al.* Arm movements induced by noninvasive optogenetic stimulation of the motor cortex in the common marmoset. *Proceedings of the National Academy of Sciences* **116**, 22844–22850 (2019).
28. Watanabe, H. *et al.* Forelimb movements evoked by optogenetic stimulation of the macaque motor cortex. *Nature Communications* **11**, 3253 (2020).
29. Wiltschko, A. B. *et al.* Mapping Sub-Second Structure in Mouse Behavior. *Neuron* **88**, 1121–1135 (2015).
30. Graziano, M. S. A., Aflalo, T. N. S. & Cooke, D. F. Arm Movements Evoked by Electrical Stimulation in the Motor Cortex of Monkeys. *Journal of Neurophysiology* **94**, 4209–4223 (2005).
31. Berger, D. J., Gentner, R., Edmunds, T., Pai, D. K. & d'Avella, A. Differences in Adaptation Rates after Virtual Surgeries Provide Direct Evidence for Modularity. *Journal of Neuroscience* **33**, 12384–12394 (2013).
32. Dyson, M., Barnes, J. & Nazarpour, K. Myoelectric control with abstract decoders. *Journal of Neural Engineering* **15**, (2018).
33. Radhakrishnan, S. M., Baker, S. N. & Jackson, A. Learning a Novel Myoelectric-Controlled Interface Task. *Journal of Neurophysiology* **100**, 2397–2408 (2008).
34. Gallego, J. A., Perich, M. G., Miller, L. E. & Solla, S. A. Neural Manifolds for the Control of Movement. *Neuron* **94**, 978–984 (2017).
35. Sanger, T. D. Bayesian Filtering of Myoelectric Signals. *Journal of Neurophysiology* **97**, 1839–1845 (2007).
36. Churchland, M. M. *et al.* Neural population dynamics during reaching. *Nature* **487**, 51–56 (2012).

37. Churchland, M. M. Neural Variability in Premotor Cortex Provides a Signature of Motor Preparation. *Journal of Neuroscience* **26**, 3697–3712 (2006).
38. Sussillo, D., Churchland, M. M., Kaufman, M. T. & Shenoy, K. V. A neural network that finds a naturalistic solution for the production of muscle activity. *Nature Neuroscience* **18**, 1025–1033 (2015).
39. Hug, F. Can muscle coordination be precisely studied by surface electromyography? *Journal of Electromyography and Kinesiology* **21**, 1–12 (2011).
40. Yang, S. C.-H., Wolpert, D. M. & Lengyel, M. Theoretical perspectives on active sensing. *Current Opinion in Behavioral Sciences* **11**, 100–108 (2016).
41. Huang, V. S., Shadmehr, R. & Diedrichsen, J. Active Learning: Learning a Motor Skill Without a Coach. *Journal of Neurophysiology* **100**, 879–887 (2008).
42. Nazarpour, K., Al-Timemy, A. H., Bugmann, G. & Jackson, A. A note on the probability distribution function of the surface electromyogram signal. *Brain Research Bulletin* **90**, 88–91 (2013).
43. Clancy, K. B., Koralek, A. C., Costa, R. M., Feldman, D. E. & Carmena, J. M. Volitional modulation of optically recorded calcium signals during neuroprosthetic learning. *Nature Neuroscience* **17**, 807–809 (2014).
44. Sadtler, P. T. *et al.* Neural constraints on learning. *Nature* **512**, 423–426 (2014).
45. Crouzier, M. *et al.* Do individual differences in the distribution of activation between synergist muscles reflect individual strategies? *Experimental Brain Research* **237**, 625–635 (2019).
46. Gallivan, J. P., Barton, K. S., Chapman, C. S., Wolpert, D. M. & Randall Flanagan, J. Action plan co-optimization reveals the parallel encoding of competing reach movements. *Nature Communications* **6**, 7428 (2015).
47. Gallivan, J. P., Logan, L., Wolpert, D. M. & Flanagan, J. R. Parallel specification of competing sensorimotor control policies for alternative action options. *Nature Neuroscience* **19**, 320–326 (2016).